Seasonal variations and profile measurements of photolysis frequencies $j(O^1D)$ and $j(NO_2)$ at the ECHO forest field site

B. Bohn,[1] R. Koppmann,[1] and F. Rohrer[1]

Received 7 November 2005; revised 21 February 2006; accepted 15 March 2006; published 17 June 2006.

[1] The Emission and Chemical Transformation of Biogenic Volatile Organic Compounds (ECHO) project investigated formation, transport, and photochemistry of biogenic organic compounds in a deciduous forest. Within the project, filterradiometers were used to measure photolysis frequencies $j(O^1D)$ ($O_3 + h\nu \rightarrow O_2 + O(^1D)$) and $j(NO_2)$ ($NO_2 + h\nu \rightarrow NO + O(^3P)$) at different levels of a tower set up in a small clearing in a forest at Jülich, Germany. The tower served as a measurement platform for instruments in two photochemistry field campaigns during the summer seasons of 2002 and 2003. Filterradiometer measurements were made throughout a complete vegetation cycle to give an extended characterization of the field site UV radiation conditions. At fully developed foliage, 3–7% of above-forest values of $j(O^1D)$ and $j(NO_2)$ were obtained close to ground at the tower clearing, dependent on external conditions. In the course of the vegetation period, these ratios remained fairly constant. After fall of leaves, photolysis frequencies increased to about 33% of above-forest values. Profile measurements in undisturbed forest showed a strong decrease of $j(NO_2)$ by about 90% within 5 m below canopy top (≈33 m) and a slowed decrease to typically 2% at ground level. At the tower clearing the decrease was more gradual reaching 50% of above-canopy values approximately 10 m below canopy top under overcast conditions. With regard to photochemical conversion of biogenic compounds we estimated that degradation of the major reactive compound isoprene within the forest by OH and O_3 was insignificant (<10%) if residence times were less than about 1 hour.

Citation: Bohn, B., R. Koppmann, and F. Rohrer (2006), Seasonal variations and profile measurements of photolysis frequencies $j(O^1D)$ and $j(NO_2)$ at the ECHO forest field site, *J. Geophys. Res.*, *111*, D12303, doi:10.1029/2005JD006856.

1. Introduction

[2] The photolyses of nitrogen dioxide and ozone,

$$NO_2 + h\nu(\lambda \leq 420\,\text{nm}) \longrightarrow O(^3P) + NO \quad (1)$$

$$O_3 + h\nu(\lambda \leq 340\,\text{nm}) \longrightarrow O(^1D) + O_2 \quad (2)$$

are important processes in tropospheric photochemistry. Secondary reactions of the electronic ground and excited state oxygen atoms are the major source of tropospheric ozone and OH radicals, respectively.

$$O(^3P) + O_2 + M \longrightarrow O_3 + M \quad (3)$$

$$O(^1D) + H_2O \longrightarrow 2\,OH \quad (4)$$

OH radicals are key species in the self-cleaning process of the atmosphere because they react with most atmospheric trace gases initiating their degradation. However, this degradation is accompanied by formation of peroxy radicals (RO_2) that can regenerate the NO_2 consumed in reaction (1).

$$RO_2 + NO \longrightarrow RO + NO_2 \quad (5)$$

Under conditions with high photochemical activity this leads to a net formation of ozone and other potentially harmful compounds as commonly observed in polluted air during the summer season. On the other hand, in the absence of RO_2, formation of O_3 following reaction (1) is balanced by reaction of NO with O_3:

$$O_3 + NO \longrightarrow O_2 + NO_2 \quad (6)$$

[3] Biogenic volatile organic compounds (BVOCs) are supposed to contribute significantly to the total reactivity and ozone formation in tropospheric air. Moreover, oxidation products of BVOCs play an important role in aerosol generation influencing cloud formation and climate. A problem concerning the impact of these compounds on

[1]Institut für Chemie und Dynamik der Geosphäre II: Troposphäre, Forschungszentrum Jülich, Jülich, Germany.

0148-0227/06/2005JD006856

Figure 1. Setup of two filterradiometers 4 m above ground at the ECHO main tower: 4 π sr $j(NO_2)$ instrument (left) and 2 π sr $j(O^1D)$ instrument (right). Shadow rings (black) limited the fields of view to one hemisphere.

tropospheric photochemistry is the uncertainty regarding the source strengths of different terrestrial ecosystems, most importantly forests, with isoprene being the most relevant reactive compound on a global scale [*Guenther et al.*, 1995; *Fuentes et al.*, 2000]. A key question for example is what fraction of different BVOCs emitted by plants are finally released into the boundary layer and what fraction is processed already within the forest by reactions with O_3, OH and NO_3 (e.g., *Makar et al.* [1999]; *Stroud et al.* [2005]).

[4] The Emission and Chemical Transformation of Biogenic Volatile Organic Compounds (ECHO) project investigated the complex process of exchange of trace gases between a forest and the planetary boundary layer. This included biological processes controlling the gas exchange between plants and air, emission and uptake of gases by soil, chemical transformations and transport phenomena within the forest as well as transport processes between the forest and the boundary layer. A wide range of measurement techniques was used to simultaneously study chemical composition, micrometeorology and photochemistry during two 5-week field campaigns in the summer seasons of 2002 and 2003 [*Ammann et al.*, 2004; *Kleffmann et al.*, 2005; *Spirig et al.*, 2005]. These campaigns were conducted in a typical European deciduous forest at Forschungszentrum Jülich, Germany (50.91°N, 6.41°E) [*Aubrun and Leitl*, 2004; *Aubrun et al.*, 2005]. Three towers were set up in the forest serving as measurement platforms.

[5] In this work we present measurements of photolysis frequencies $j(NO_2)$ and $j(O^1D)$ at the ECHO main tower and the surrounding forest. $j(NO_2)$ and $j(O^1D)$ are rate constants quantifying reactions (1) and (2) in terms of the loss rate of the precursor molecule and the formation rate of the photoproduct, respectively.

$$j(NO_2) = -\frac{d[NO_2]}{dt}\frac{1}{[NO_2]} \tag{7}$$

$$j(O^1D) = \frac{d[O^1D]}{dt}\frac{1}{[O_3]} \tag{8}$$

The notation $j(O^1D)$ was preferred rather than $j(O_3)$ because ozone photolysis is also leading to ground state $O(^3P)$ in the tropospheric wavelength range. Besides the chemical definitions in equations (7) and (8), photolysis frequencies can also be expressed in terms of radiometric and molecular quantities, e.g., in the case of $j(O^1D)$:

$$j(O^1D) = \int \sigma(O_3)\phi(O^1D)F_\lambda(\lambda)d\lambda \tag{9}$$

Here $\sigma(O_3)$ is the absorption cross section of ozone, $\phi(O^1D)$ is the quantum yield of $O(^1D)$ and F_λ is the spectral actinic photon flux, all dependent on wavelength. Spectral actinic flux can be measured absolutely using spectroradiometers with appropriate input optics [e.g., *Hofzumahaus et al.*, 1999]. However, these measurements are complex and instruments are unwieldy. Filterradiometers use similar input optics and broadband detection of spectral actinic flux in selected ranges imitating the relative wavelength dependence of the product $\sigma(\lambda)\ \phi(\lambda)$ of a specific photolysis process. Ideally this produces an output signal that is proportional to the photolysis frequency of the desired process. The instruments are lightweight and need little maintenance making them suitable for sites difficult to access.

[6] The filterradiometer measurements within the ECHO project were extended beyond the intensive campaigns covering the complete vegetation period to provide information on diurnal and seasonal dependencies of UV radiation conditions at the field site. Moreover, the flexibility of the instruments allowed for profile measurements at the tower clearing and the nearby forest. Both aspects complemented spectroradiometer measurements that were conducted during the campaigns within and above the forest. These measurements are described in a separate paper [*Bohn*, 2006].

2. Experimental and Site Description

2.1. Filterradiometers

[7] As briefly explained in the introduction, filterradiometers measure integrated spectral actinic flux in wavelength ranges selected to reproduce specific photolytic processes. $j(NO_2)$ and $j(O^1D)$ instruments are available commercially (Metcon GmbH, Glashütten, Germany). The input optics consist of quartz domes covering a 2 π sr solid angle with direction independent sensitivity. The design and data evaluation of filterradiometers is described in detail elsewhere [*Junkermann et al.*, 1989; *Volz-Thomas et al.*, 1996; *Bohn et al.*, 2004]. Figure 1 shows two instruments set up at the ECHO tower.

Figure 2. ECHO main tower and forest clearing. Platforms marked levels of 18, 27, and 36 m. Elevator tracks are visible on the right-hand side of the construction.

[8] All instruments were characterized in terms of spectral sensitivity and angular response. Absolute calibrations were made in 2002 and 2003 prior to installation of the instruments at the tower by intercomparisons with an actinic flux spectroradiometer with PTB traceable spectral calibration [*Hofzumahaus et al.*, 1999]. For the calculation of photolysis frequencies from the actinic flux spectra, selected data sets of absorption cross sections and quantum yields of the corresponding photolysis processes were used [*Malicet et al.*, 1995; *Merienne et al.*, 1995; *Troe*, 2000; *Matsumi et al.*, 2002]. Recent comparisons show that the spectroradiometric method of deriving photolysis frequencies (equation (9)) was consistent with actinometric determinations within 10% or better [*Shetter et al.*, 2003; *Hofzumahaus et al.*, 2004] supporting the accuracy of the molecular data from literature.

[9] The filterradiometers provided an analog output signal that was recorded with a time resolution of 5–7 s during calibration and the tower measurements. For $j(NO_2)$ there was a linear relationship between the output signals and photolysis frequencies obtained with the spectroradiometer. Calibration factors were derived by linear regressions for each instrument. With regard to the spectroradiometer reference, standard deviations of typically 3% remained at solar zenith angles (χ) less than 80°. These deviations were attributable to an imperfect synchronization of the instruments. The accuracy of $j(NO_2)$ from the filterradiometer measurements was therefore estimated similar to that of the spectroradiometer ($\approx$10%).

[10] For $j(O^1D)$ conversion of the output signals to photolysis frequencies was more complicated because of the strong variability of spectral actinic flux in the UV-B. This was taken into account by instrument specific correction factors as a function of solar zenith angle and ozone column that were calculated based on simulated solar actinic flux spectra [*Bohn et al.*, 2004]. The correction factors were parameterized for each instrument and calculated using ozone columns from satellite observations (NASA Earth probe, TOMS). After application of the corrections, calibration factors were determined by linear regression using the spectroradiometer data as a reference. The remaining standard deviations were gradually increasing with solar zenith angle between typically 3% at $\chi \leq 45°$, 5% in a range $60° \leq \chi \leq 70°$ and 9% in a range $70° \leq \chi \leq 80°$. The scatter at small solar zenith angles was again mainly attributed to imperfect synchronization while the increase with solar zenith angle was caused by the increasing uncertainty of the correction procedure with regard to ozone column. The accuracy of $j(O^1D)$ filterradiometer measurements was therefore estimated 10% for $\chi \leq 70°$ as in the case of $j(NO_2)$ and 15% for $70° \leq \chi \leq 80°$.

[11] Moreover, it should be noted that $j(O^1D)$ was temperature dependent mainly caused by a temperature dependence of the $O(^1D)$ quantum yields (*Matsumi et al.* [2002] and references therein). The photolysis frequencies reported in this work were calculated for a temperature of 298 K to keep separated the effects of foliage and external temperature variations. However, in studies on photochemistry the actual temperature should be considered, e.g., by using a recently published parameterization [*Bohn et al.*, 2004].

2.2. ECHO Main Tower Measurements

[12] The ECHO main tower was assembled from a 36 m crane (no extension arm), three platforms mounted at 18, 27, and 36 m levels, and an elevator (Figure 2). The tower was situated in a small, almost circular clearing with a diameter of about 15 m (gradually decreasing within the two vegetation periods) at a small road leading through the forest. The clearing was surrounded mainly by large beech trees with canopy heights ranging up to 35 m.

[13] Filterradiometers were mounted at three different levels, namely at 38, 19, and 4 m. At 38 m above-forest measurements were made with $j(NO_2)$ and $j(O^1D)$ filterradiometers using a 2 m vertical extension at the highest platform to obtain full view of the upper hemisphere. At 19 m a $j(O^1D)$ instrument was installed in easterly direction 2.5 m from the tower center (1.8 m from the tower edge). At 4 m another combination of $j(NO_2)$ and $j(O^1D)$ filterradiometers was used that was installed 2.5 m from the tower center in westerly direction (1.8 m from the tower edge, Figure 1). Caused by the proximity of the tower, about 10% of the field of view was blocked by the tower for the instruments at the 19 and 4 m levels. Measurements were made on a total of 143 days and 190 days in 2002 and 2003, respectively. Autumn/early winter data were collected in 2002, late winter/spring data in 2003. During the periods 9 July to 25 July 2002 and 5 July to 2 August 2003 measurements at the lowest level (4 m) were suspended to use the filterradiometers at the tower elevator close to an instrument measuring OH and HO_2 radical concentrations [*Kleffmann et al.*, 2005].

[14] At the highest and the lowest level the $4\pi\, j(NO_2)$ measurements provided information on the upwelling radiation and the corresponding photolysis frequencies. Fairly constant ratios of upwelling and downwelling values of about 4% and 10% were obtained at 4 and 38 m, respectively. However, these ratios were considered inaccurate

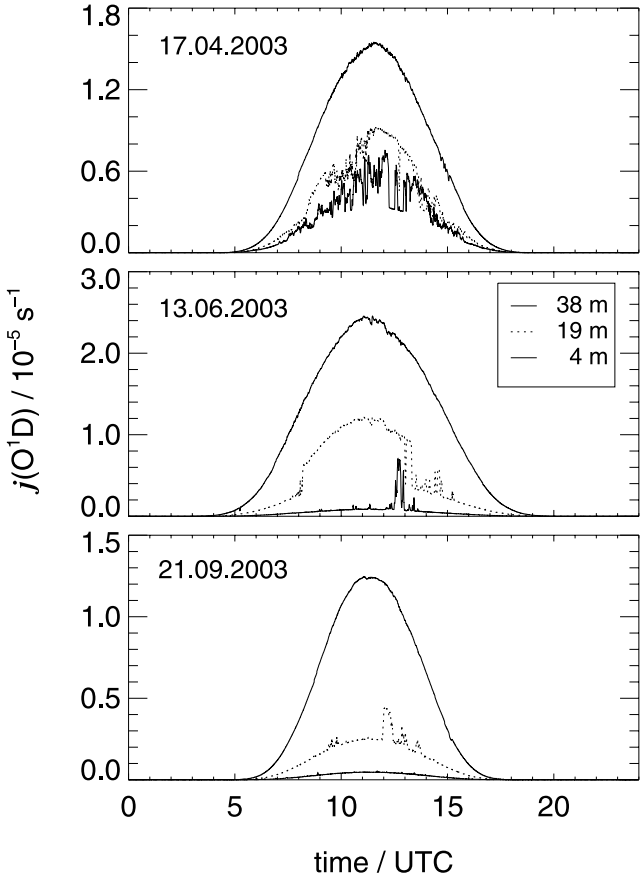

Figure 3. Diurnal variations of $j(O^1D)$ photolysis frequencies at different levels of the tower on three clear-sky days of different seasons. From top to bottom: 38, 19, and 4 m in each panel. No foliage was present on 17 April 2003. Foliage was fully developed on 13 June and 21 September 2003. Note the different y axis scales.

because lower hemisphere measurements were influenced locally by artificial bright surfaces and a slight crosstalk to the upper hemisphere caused by the limited size of the shadow rings (see Figure 1). The data were therefore not used in the following and the contribution of upwelling radiation was neglected. Literature data on the albedo of natural surfaces covered by vegetation usually ranged around 1–4% in the UV generally decreasing with decreasing wavelength [*Feister and Grewe*, 1995; *Webb et al.*, 2004].

2.3. Profile Measurements

[15] Profile measurements were made with a further, battery-powered $j(NO_2)$ filterradiometer. At the main tower the elevator with a 2.5 m extension arm pointing toward northeasterly (NE) or northwesterly (NW) directions were used to carry out the measurements at distances of 5 m from the tower center. The traveltime between ground level and tower top, and vice versa, was about 2 min. Profile measurements in the forest were made using a movable platform mounted on a truck that could be extended up to 40 m, i.e., above canopy top. A winch was used to lift and lower the filterradiometer within about 2 min. Forest measurements were made at two locations about 20 and 30 m away from the tower in southeasterly (SE) direction where the influence of the clearing was insignificant.

3. Results and Discussion

3.1. Continuous Measurements at the Tower

3.1.1. Diurnal Variations

[16] Figure 3 shows examples of diurnal variations of $j(O^1D)$ at different levels under clear-sky conditions of different seasons. Above the forest a strong seasonal dependence of $j(O^1D)$ on the elevation of the sun can be recognized as expected for a process assigned to the UV-B range that is strongly influenced by absorption by stratospheric ozone.

[17] No foliage was present on 17 April 2003 (Figure 3, top), i.e., photolysis frequencies below forest top were reduced by the influence of leafless branches and trunks of the surrounding trees. In a forest of reasonable extension these opaque objects were effectively obstructing the sky toward large zenith angles explaining the substantial reduction of photolysis frequencies already in the absence of foliage. The strong fluctuations at the lower levels can be explained by shadows, i.e., by rapid variations of the fraction of direct sunlight received at the measurement sites.

[18] At fully developed foliage (Figure 3, middle and bottom) there was a strong seasonal effect at the medium level (19 m) with direct sunlight contributing strongly for longer periods close to summer solstice (13 June) but rarely close to equinox (21 September). At the lowest level (4 m) the presence of foliage led to a much stronger reduction of photolysis frequencies. Moreover, variations caused by direct sunlight were very rare, causing sharp peaks of limited amplitude except for short periods at high elevations of the sun (middle panel). The peak patterns were found to vary from day to day explainable by mainly small gaps in the foliage being responsible for the variations. For $j(NO_2)$ a similar behavior was found qualitatively. However, because NO_2 photolysis takes place in the UV-A range, seasonal variations were less pronounced above canopy and contributions of direct sunlight were greater than in the case of $j(O^1D)$.

[19] Under overcast conditions the situation was more complex above the forest but simpler regarding the influence of the forest. Caused by changes in cloud thickness, $j(O^1D)$ and $j(NO_2)$ exhibited strong and unpredictable variations above canopy. However, as is evident from Figures 4 and 5 for both photolysis frequencies, diurnal variations at different levels were similar except for scaling factors. The scaling factors depended on the presence or absence of foliage but showed no further dependence on season. Moreover, they were similar for $j(O^1D)$ and $j(NO_2)$. This behavior was in accord with similar sky radiance distributions in UV-A and UV-B ranges under overcast conditions and a foliage being virtually opaque for the complete UV range. Spectroradiometer measurements from the campaign periods confirmed this result for forest and clearing locations [*Bohn*, 2006].

[20] From a selected data set assembled from 14 and 11 completely overcast days in 2002 and 2003, respectively, linear correlation coefficients $r \geq 0.97$ were obtained for photolysis frequencies at different levels. Mean ratios below/above canopy were ranging between 6.2% and 7.2% for

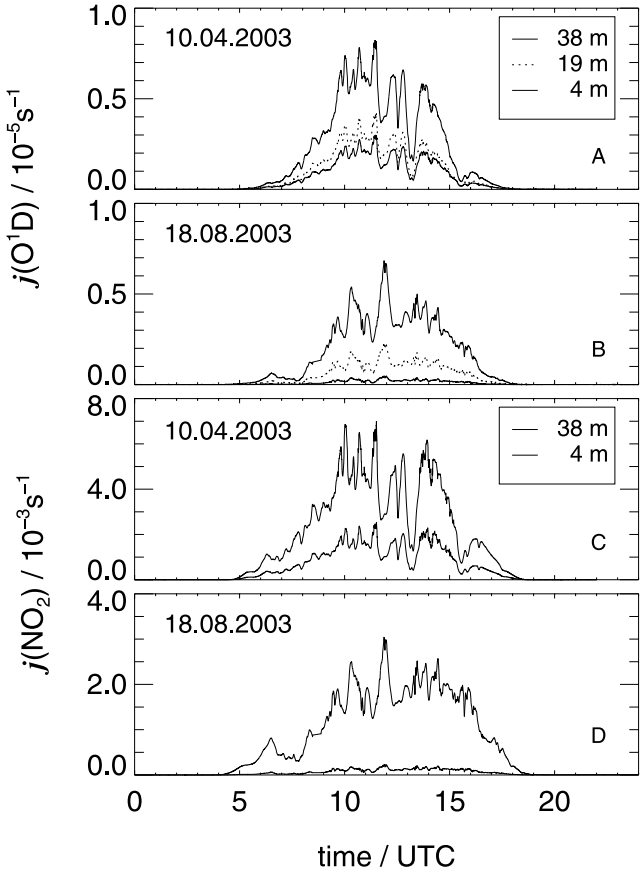

Figure 4. Diurnal variations of $j(O^1D)$ and $j(NO_2)$ at different levels of the tower on two overcast days of different seasons. From top to bottom: 38, 19, 4 m (Figures 4a and 4b) and 38 and 4 m (Figures 4c and 4d). No foliage was present on 10 April 2003. Foliage was fully developed on 18 August 2003.

the 4 m level and around 32% for the 19 m level. In the absence of foliage these ratios increased to about 33% and 50%, respectively. Moreover, test measurements showed that during the winter season differences between the clearing and the nearby forest were insignificant. A summary of the results is given in Table 1.

[21] A similar analysis for clear-sky days or days with broken cloud cover was considered unsuitable because of the variable and sporadic influence of direct sunlight. In section 3.1.2 we therefore used daily integrals of photolysis frequencies to include all measurement days in an overview of seasonal variations. A more detailed analysis of the time-dependent effects observed on clear-sky days is given elsewhere [*Bohn*, 2006].

3.1.2. Seasonal Variations

[22] By integrating photolysis frequencies over a day, a quantity was obtained corresponding to the number of photolyses a precursor molecule experienced during one day. These photolysis numbers were denoted S in the following:

$$S(NO_2) = \int_{day} j(NO_2)dt \quad (10)$$

$$S(O^1D) = \int_{day} j(O^1D)dt \quad (11)$$

In Figure 6, $S(O^1D)$ and $S(NO_2)$ were plotted for different tower levels as a function of the day of the year. There was a strong variability mainly caused by day-to-day changes of cloud cover. The envelopes of the data above canopy showed different shapes for $S(O^1D)$ and $S(NO_2)$ as expected from the different dependencies of the photolysis frequencies on solar zenith angle. Moreover, absolute numbers of $S(O^1D)$ and $S(NO_2)$ differed by a factor 500 or more. For an ozone molecule this means that photolysis to $O(^1D)$ took place less than once a day. On the other hand, an NO_2 molecule was subject to photolysis up to 300 times a day, assuming instantaneous regeneration by reactions (5) and (6).

[23] Within the forest photolysis numbers were substantially smaller. At the 4 m level at summer solstice $S(O^1D)$ and $S(NO_2)$ merely ranged around 0.03 and 6, respectively. Because the vegetation period was shifted against the

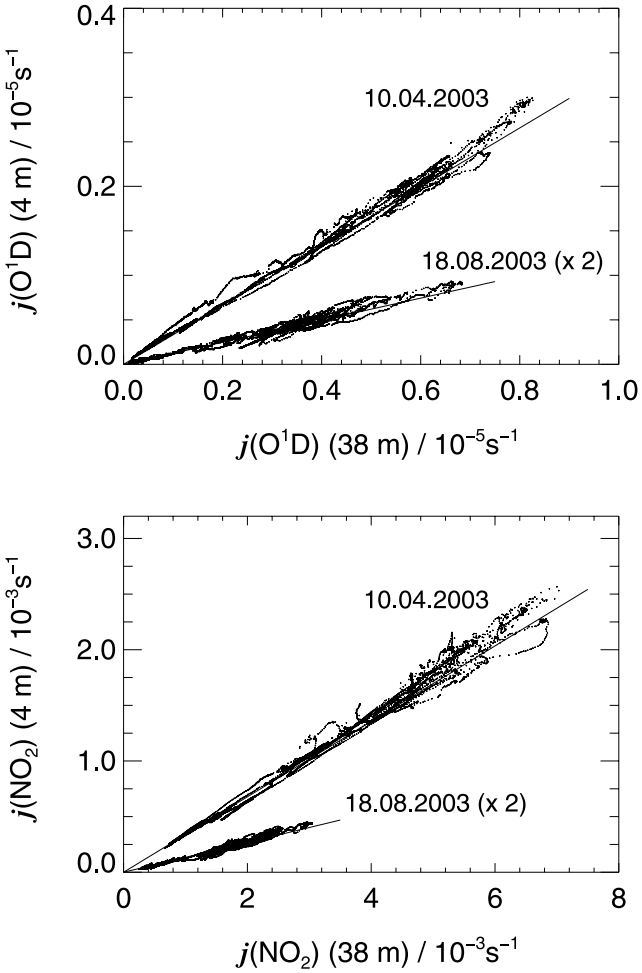

Figure 5. Correlation of $j(O^1D)$ and $j(NO_2)$ at 4 and 38 m tower levels on two overcast days of different seasons. No foliage was present on 10 April 2003 (N = 6405). Foliage was fully developed on 18 August 2003 (N = 6679). Solid lines indicate the mean results for overcast conditions listed in Table 1.

Table 1. Linear Correlation Coefficients and Mean Ratios of Photolysis Frequencies Relative to Above Forest Values on Completely Overcast Days[a]

Instrument	Correlation Coefficient	Above Canopy Ratio
	Foliage	
	2002 (14 days, N = 89000)	
$j(NO_2)$ 4 m	0.980	0.072 ± 0.008
$j(O^1D)$ 4 m	0.992	0.071 ± 0.009
$j(O^1D)$ 19 m	0.995	0.333 ± 0.027
	2003 (11 days, N = 72500)	
$j(NO_2)$ 4 m	0.970	0.067 ± 0.009
$j(O^1D)$ 4 m	0.991	0.062 ± 0.013
$j(O^1D)$ 19 m	0.995	0.315 ± 0.037
	No Foliage	
	2002 (7 days Autumn, N = 26500)	
$j(NO_2)$ 4 m	0.983	0.306 ± 0.021
$j(O^1D)$ 4 m	0.994	0.335 ± 0.070
$j(O^1D)$ 19 m	0.993	0.534 ± 0.141
	2003 (3 days Spring, N = 22000)	
$j(NO_2)$ 4 m	0.987	0.339 ± 0.030
$j(O^1D)$ 4 m	0.994	0.323 ± 0.033
$j(O^1D)$ 19 m	0.996	0.474 ± 0.028

[a]Data points at solar zenith angles >80° were not considered. Error bars are 1σ.

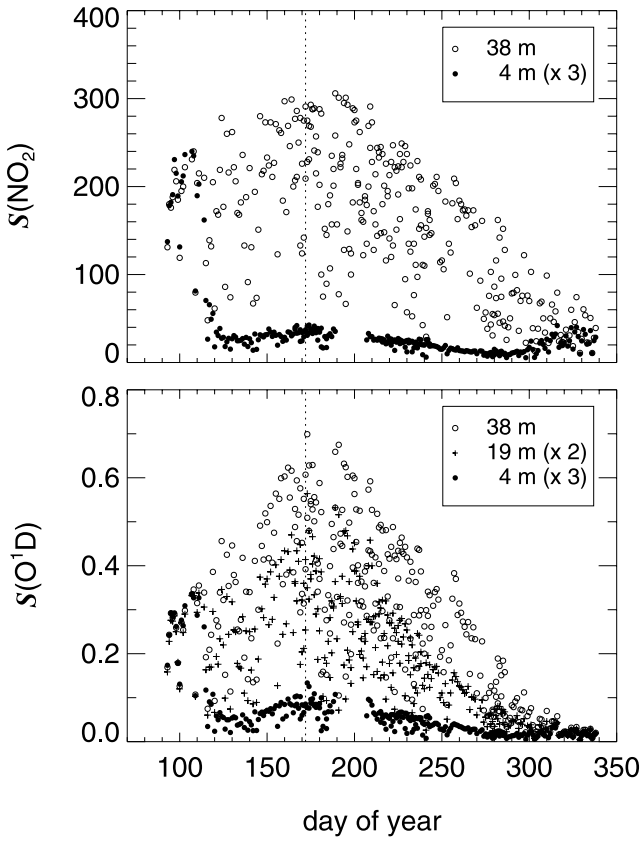

Figure 6. Seasonal variation of daily integrals S of photolysis frequencies at different levels (equations (10) and (11)). To improve visibility, data from 4 and 19 m levels were scaled by factors 3 and 2, respectively. The dashed line indicates the date of summer solstice.

annual cycle of solar radiation the smallest S within the forest were observed during autumn right before the fall of leaves, while the greatest values were found during springtime just before sprout of leaves.

[24] In Figure 7, ratios $S_r = S/S_{38\,m}$ relative to above-forest values were plotted. Here part of the scatter induced by clouds that dominated Figure 6 cancels out making seasonal effects more clear. The gap in the data set at 4 m indicates the periods of intensive campaigns where the instruments were used otherwise. Formation of foliage during springtime was completed remarkably quick within about 10 days. The fall of leaves during autumn took about 20 days.

[25] At the 19 m level there was a minimum recognizable at around equinox (day 266) while the greatest values in the presence of foliage were obtained at around summer solstice. However, as described in section 3.2.1, these variations did not apply for overcast conditions. Under clear-sky conditions ratios were greatest at around summer solstice because the instrument was receiving direct sunlight at periods around noon when the contribution of direct sunlight was at a maximum. On the other hand, the autumn minimum was reached when direct sunlight was still important above the canopy but rarely reached the instrument because of the lower elevation of the sun.

[26] At the 4 m level clear-sky day ratios were always below the ratios obtained on overcast days because above-forest values were at all seasons benefiting more from direct sunlight than within the forest. In particular this applied for $j(NO_2)$ where the contribution by direct sunlight was high also during the winter season, i.e., in the absence of foliage.

3.2. The $j(NO_2)$ Profile Measurements

3.2.1. Main Tower Clearing

[27] Figure 8 shows the result of profile measurements at the tower under overcast conditions. Ratios $j_r(NO_2) = j(NO_2)/j(NO_2)_{38m}$ of photolysis frequencies relative to

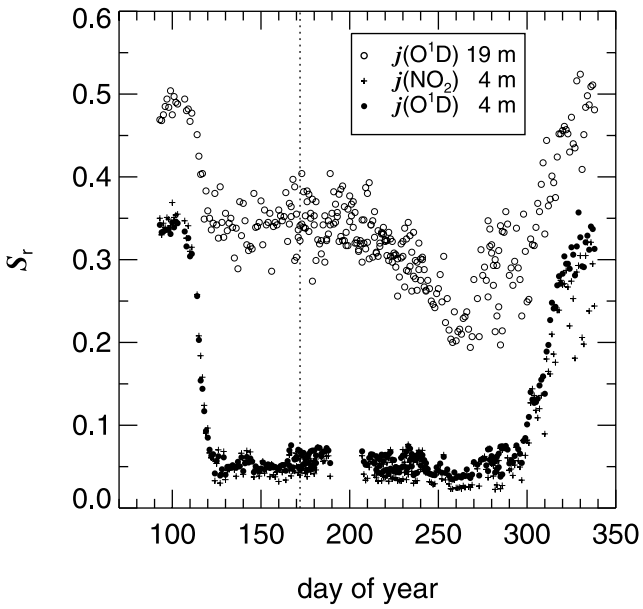

Figure 7. Seasonal variation of ratios $S_r = S/S_{38\,m}$ of daily integrals of photolysis frequencies at different levels relative to above-canopy values. The dashed line indicates the date of summer solstice.

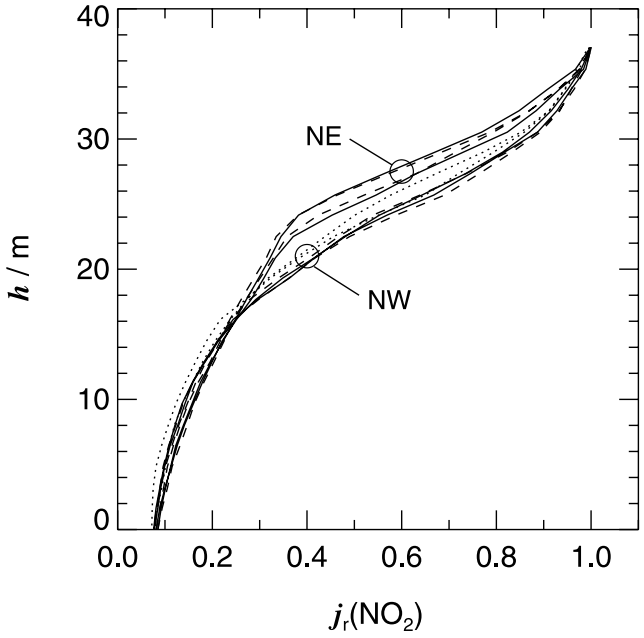

Figure 8. Profiles of $j_r(NO_2) = j(NO_2)/j(NO_2)_{38m}$ at the tower under overcast conditions. Each profile consisted of ascending and descending parts. Different runs are indicated by different line styles. Legends denote different positions: 5 m NE (two profiles) and 5 m NW (three profiles) with respect to tower center.

above-forest values were plotted as a function of altitude h. Ascending and descending runs and repeated measurements on that day showed good reproducibility. This can be explained by a constant relative sky radiance distribution producing profiles independent of time. Moreover, because of the similar scaling factors for $j(NO_2)$ and $j(O^1D)$ at selected levels under overcast conditions (Table 1), $j(O^1D)$ profiles were expected to look similar. Differences were obtained with the extension arm pointing toward NE or NW directions. This can be explained by a stronger obstruction of the sky by a large tree dominating the NE with the instrument almost touching branches during the runs. On the other hand, ratios at ground level were smaller in NW direction where the extension of the clearing was slightly smaller. Values at 19 and 4 m were in reasonable agreement with the long-term measurements at these levels (Table 1) despite horizontal distances of 7 m between measurement sites.

[28] Under clear-sky and broken cloud conditions the situation was more complex. Figure 9 shows measurements taken on a clear-sky day close to summer solstice (16 June 2003). Here rapid changes of the ratios were found upon small changes of elevation. Moreover, the profiles were time-dependent, i.e., dependent on solar zenith and azimuth angles. Basically the data can be explained by rapid variations between two extreme profiles lying at higher and lower values compared to the overcast profiles. The extreme profiles corresponded to exposure and nonexposure to direct sunlight and the range was defined by the contribution of direct sunlight above the forest. For example, at 1040 UTC (about 1 hour before local noon) solar zenith and azimuth angles allowed direct sunlight to pass the clearing gap to the radiometer at all elevations except for the lowermost about 4 m. Moreover at that time of day the contribution of direct sunlight was greatest compared to the other profiles (see section 3.2.3 for more details). Compared to Figure 9, clear-sky $j(O^1D)$ profiles were expected to exhibit a less pronounced variability caused by the lower contribution of direct sunlight to $j(O^1D)$.

3.2.2. Undisturbed Forest

[29] Profiles in undisturbed forest were measured at conditions with broken cloud cover with direct sunlight being present sporadically because the period for the measurements could not be selected as freely as for the tower measurements. Figure 10 shows the result of four measurements at two different locations close to the tower clearing (20–30 m) but unaffected by the clearing. Spot check measurements showed that the transition between undisturbed forest and the clearing occurs quickly within a range of about 10 m that can be explained by the vertical extension of the canopy.

[30] Compared to the tower profiles the reduction of photolysis frequencies within the first few meters was much more pronounced. Some 5 m below the canopy top photolysis frequencies dropped by about 90%. This level marked the lower limit of the densest part of canopy. Below there

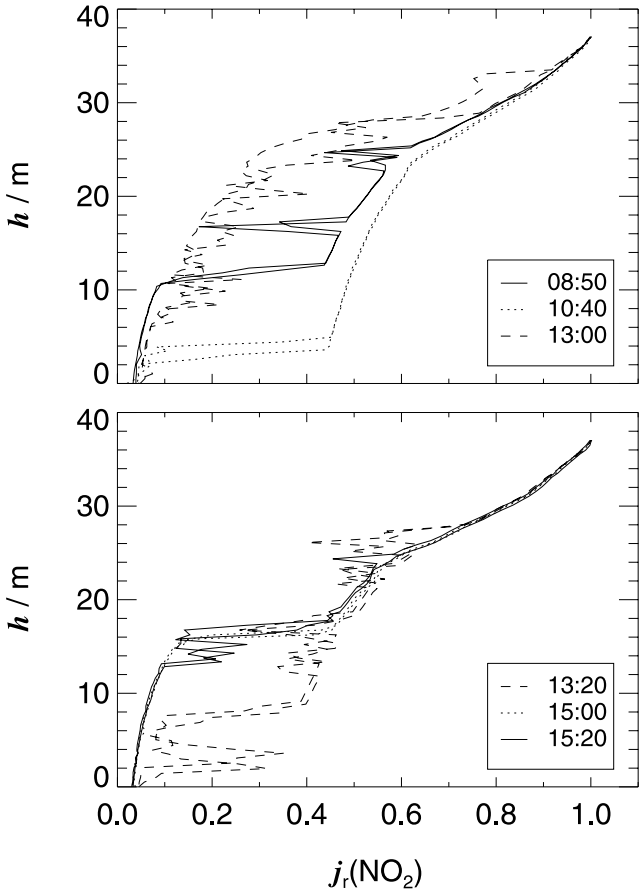

Figure 9. $j_r(NO_2)$ profiles at the tower (5 m NW from tower center) under clear-sky conditions at different times of day (16 June 2003). Each profile consisted of ascending and descending runs. Rapid variations were caused by changing contributions of direct sunlight. Time data are UTC.

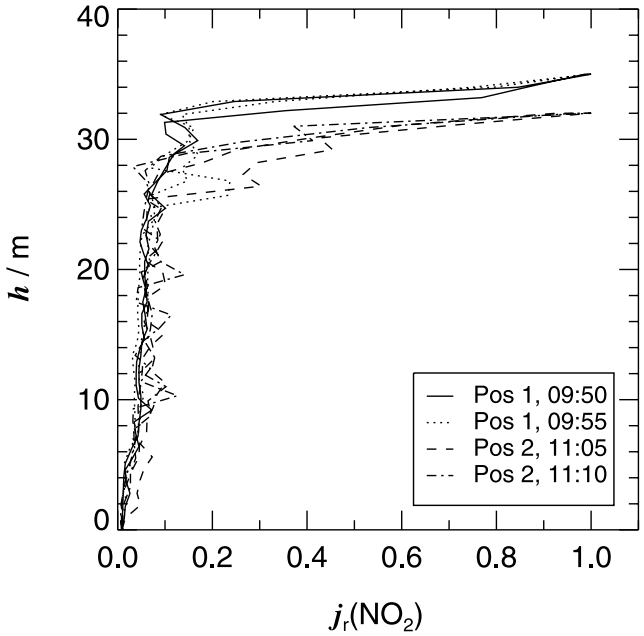

Figure 10. The $j_r(NO_2)$ profiles in undisturbed forest under cloudy conditions. A 40 m lifting platform and a winch were used for these measurements. Two positions (Pos 1, Pos 2) were chosen at distances of about 20 and 30 m from the tower clearing (SE). Each profile consisted of ascending and descending runs. Rapid variations were caused by sporadic influence of direct sunlight. Time data are UTC.

were few branches carrying leaves. Accordingly photolysis frequencies decreased slowly in a range between 25 and 10 m. Below there was a further decrease caused by a layer of leaves from young trees present at some places. At ground level some 1% of external values were found. This ratio was in accordance with spectroradiometer measurements close to ground level in undisturbed forest that lay in a 1–3% range of above-forest values [*Bohn*, 2006]. Moreover, it should be noted that because of the significant differences between the undisturbed forest and the clearing the diurnal and seasonal variations described in section 3.1 could not be translated to the undisturbed forest.

3.2.3. Idealized Profiles

[31] Mean overcast profiles were calculated for the tower clearing and the forest. To improve comparability, a normalized altitude $h_r = h/h_f$ was introduced where h_f corresponds to the altitude of the forest top at the different locations. Figure 11 shows the mean profiles together with parameterizations describing idealized profiles based on the following equation:

$$j_r^{\text{overcast}}(h_r) = \exp\left\{\sum_n a_n h_r^n\right\} \quad \text{with } h_r \le 1 \tag{12}$$

The polynomial coefficients a_n were obtained by fitting equation (12) to the mean profiles. They are listed in Table 2. These profiles are recommended for use in model studies regarding photochemistry in the forest and the clearing. For the idealized forest profile $j_r^{\text{overcast}}(h_r = 0)$ was adjusted to 0.02 corresponding to an averaged value obtained at different forest locations close to ground level under overcast conditions [*Bohn*, 2006].

[32] In the presence of direct sunlight, profiles may range between two extremes as already mentioned in section 3.2.1.

$$j_r^{\text{shadow}} = j_r^{\text{overcast}}(1 - \alpha_{\text{direct}}) \tag{13}$$

$$j_r^{\text{sun}} = j_r^{\text{overcast}}(1 - \alpha_{\text{direct}}) + \alpha_{\text{direct}} \tag{14}$$

[33] The indices shadow and sun denote conditions where no direct sunlight and total direct sunlight were received, respectively. α_{direct} is the photolysis frequency fraction above canopy attributable to direct sunlight. During the intensive campaigns these contributions of direct sunlight were measured above the forest [*Bohn*, 2006]. In Figure 11 the profiles corresponding to equations (13) and (14) were plotted for the clearing assuming $\alpha_{\text{direct}} = 0.3$. Obviously, the larger extreme j_r^{sun} is fairly unlikely at low sun or small h_r. On the other hand, j_r^{sun} prevails at high solar elevation for h_r close to one (see Figure 9 for comparison).

[34] Spectroradiometer measurements showed that compared to overcast conditions a significantly lower and time-dependent fraction of above canopy diffuse sky radiation was received in the clearing under clear-sky conditions [*Bohn*, 2006]. However, given the uncertainties of the actual, time-dependent contribution of direct sunlight at the tower, equations (13) and (14) were considered reasonable approximations.

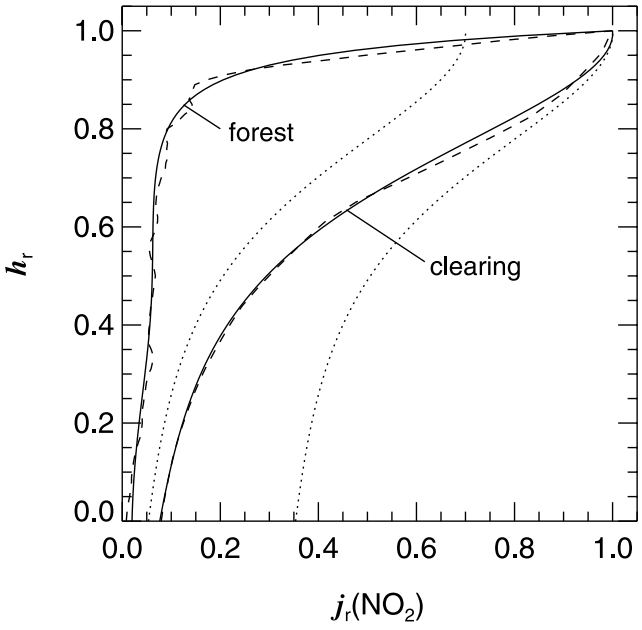

Figure 11. Measured mean tower and forest $j_r(NO_2)$ as a function of a normalized canopy height h_r (dashed lines) and idealized profiles according to equation (12) (solid lines). The dotted lines indicate extreme tower profiles in the presence of direct sunlight showing the simulated radiometer receiving full (right) or no (left) direct Sun ($\alpha_{\text{direct}} = 0.3$, equations (13) and (14)).

Table 2. Polynomial Coefficients for a Parameterization of Relative Photolysis Frequency Profiles Under Overcast Conditions Equation (12)

Profile	a_0	a_1	a_2	a_3	a_4
Forest	−3.91	0.97	15.35	−38.87	26.46
Tower	−2.57	2.42	−1.08	5.28	−4.05

3.3. Photochemistry

[35] The mean $j(NO_2)$ profiles of Figure 11 indicate a strong reduction of photolysis frequencies within the forest. On average 10% of above-forest values were observed below canopy top (≈33 m) and 4% below the densest part of the canopy (≈28 m). Assuming a linear relationship between OH concentrations and photolysis frequencies as commonly observed in field campaigns, it can be concluded that photochemical degradation of BVOCs by OH is slowed down accordingly. Thus the lifetime of BVOCs with regard to reaction with OH is increased by a factor of about 25 below canopy.

[36] Isoprene was found to be the major reactive BVOC at the ECHO site with typical maximum concentration of 2–4 ppbV observed at the top of the tower during the day [*Spirig et al.*, 2005]. The local sources of isoprene were single oak trees (Quercus robur) and stands of oak in the surroundings. Isoprene was emitted during daytime by the oak leaves dependent on the presence of photosynthetic active radiation (PAR) and temperature. The total concentrations of monoterpenes from beech, birch and scattered spruce typically ranged around 10% of isoprene concentrations [*Spirig et al.*, 2005].

[37] Above the forest typically $5 \times 10^6 cm^{-3}$ of OH were observed around noon on a clear-sky day during the 2003 ECHO campaign (A. Hofzumahaus, private communication, 2005). For isoprene this means that the lifetime was increased from 30 min above the forest to 8 h below canopy. In this calculation also reaction with O_3 at a typical concentration of 50 ppbV was considered using recommended rate constants for the isoprene + OH ($1.0 \times 10^{-10} cm^3 s^{-1}$) and isoprene + O_3 ($1.3 \times 10^{-17} cm^3 s^{-1}$) reactions [*Atkinson et al.*, 2004]. Under these conditions ozone accounted for 44% of isoprene degradation below canopy.

[38] Defining a 10% reduction substantial, isoprene degradation within the forest was significant at mean residence times exceeding 50 min. Measurements showed a quick decline of isoprene concentrations when biogenic production ceased toward the evening indicating an actual residence time on the order of 30 min or less. Thus degradation of isoprene within the forest was considered negligible making the forest a net source of virtually all emitted isoprene for the boundary layer above the forest. However, for other BVOCs reacting more rapidly with O_3 the situation may be different. The potential role of NO_3 radicals as a daytime reactant within the forest is addressed elsewhere [*Bohn*, 2006].

4. Conclusions

[39] In this work UV radiation conditions at the main measurement site of the ECHO project were investigated based on filterradiometer long-term and profile measurements of $j(NO_2)$ and $j(O^1D)$. In the presence of foliage daily means of photolysis frequencies close to ground level were ranging between 3% and 7% of above-forest values dependent on season and external conditions. Under overcast conditions similar attenuation factors were found for $j(NO_2)$ and $j(O^1D)$. Caused by gaps in the canopy the effects of the foliage were more complex in the presence of direct sunlight. Seasonal variations can be explained qualitatively by the varying contributions of direct sunlight dependent on altitude, wavelength range and elevation of the sun.

[40] Profile measurements showed that in the forest photolysis frequencies were well below 10% of above-forest values except for the uppermost part (≈5 m) of the canopy. In the clearing the decrease of photolysis frequencies was more gradual typically reaching 50% of above-forest values 10 m below canopy top. However, close to ground level conditions at the tower were considered similar to mean forest conditions characterized by a substantial decrease of photolysis frequencies. This decrease is expected to limit the production of reactive radicals and thus chemical conversion of BVOCs and other trace gases within the forest. Degradation of isoprene within the forest is estimated insignificant if mean residence times are below 1 hour.

[41] **Acknowledgments.** The authors thank A. Hofzumahaus for useful discussions. Financial support of the ECHO project by the German Bundesministerium für Bildung und Forschung under grant 07ATF47 is gratefully acknowledged.

References

Ammann, C., C. Spirig, A. Neftel, M. Steinbacher, M. Komenda, and A. Schaub (2004), Application of PTR-MS for measurements of biogenic VOC in a deciduous forest, *Int. J. Mass Spectrom.*, *239*, 87–101.

Atkinson, R., D. L. Baulch, R. A. Cox, J. N. Crowley, R. F. Hampson, R. G. Hynes, M. E. Jenkin, M. J. Rossi, and J. Troe (2004), Evaluated kinetic and photochemical data for atmospheric chemistry: part 1 - Gas phase reactions of Ox, HOx, NOx and SOx species, *Atmos. Chem. Phys.*, *4*, 1461–1738.

Aubrun, S., and B. Leitl (2004), Development of an improved physical modelling of a forest area in a wind tunnel, *Atmos. Environ.*, *38*, 2797–2801.

Aubrun, S., R. Koppmann, B. Leitl, M. Möllmann-Coers, and A. Schaub (2005), Physical modelling of a complex forest area in a wind tunnel: Comparison with field data, *Agric. For. Meteorol.*, *129*, 121–135.

Bohn, B. (2006), Solar spectral actinic flux and photolysis frequency measurements in a deciduous forest during ECHO, *J. Geophys. Res.*, doi:10.1029/2005JD006902, in press.

Bohn, B., A. Kraus, M. Müller, and A. Hofzumahaus (2004), Measurement of atmospheric $O_3 \rightarrow O(^1D)$ photolysis frequencies using filterradiometry, *J. Geophys. Res.*, *109*(D16), D10S90, doi:10.1029/2003JD004319.

Feister, U., and R. Grewe (1995), Spectral albedo measurements in the UV and visible region over different types of surfaces, *J. Photochem. Photobiol.*, *62*, 736–744.

Fuentes, J. D., et al. (2000), Biogenic hydrocarbons in the atmospheric boundary layer: A review, *Bull. Am. Meteorol. Soc.*, *81*, 1537–1575.

Guenther, A., et al. (1995), A global model of volatile organic compound emissions, *J. Geophys. Res.*, *100*, 8873–8892.

Hofzumahaus, A., A. Kraus, and M. Müller (1999), Solar actinic flux spectroradiometry: A technique for measuring photolysis frequencies in the atmosphere, *Appl. Opt.*, *38*, 4443–4460.

Hofzumahaus, A., et al. (2004), Photolysis frequency of O_3 to $O(^1D)$: Measurement and modelling during the international photolysis frequency measurement and modeling intercomparision (IPMMI), *J. Geophys. Res.*, *109*(D8), D08S90, doi:10.1029/2003JD004333.

Junkermann, W., U. Platt, and A. Volz-Thomas (1989), A photoelectric detector for the measurement of photolysis frequencies of ozone and other atmospheric molecules, *J. Atmos. Chem.*, *8*, 203–227.

Kleffmann, J., T. Gavriloaiei, A. Hofzumahaus, F. Holland, R. Koppmann, L. Rupp, E. Schlosser, M. Siese, and A. Wahner (2005), Daytime formation of nitrous acid: A major source of OH radicals in a forest, *Geophys. Res. Lett.*, *32*, L05818, doi:10.1029/2005GL022524.

Makar, P. A., J. D. Fuentes, D. Wang, R. M. Staebler, and H. A. Wiebe (1999), Chemical processing of biogenic hydrocarbons within and above a deciduous forest, *J. Geophys. Res.*, *104*, 3581–3603.

Malicet, J., D. Daumont, J. Charbonnier, C. Parisse, A. Chakir, and J. Brion (1995), Ozone UV spectroscopy II: Absorption cross-sections and temperature dependence, *J. Atmos. Chem.*, *21*, 263–273.

Matsumi, Y., F. J. Comes, G. Hancock, A. Hofzumahaus, A. J. Hynes, M. Kawasaki, and A. R. Ravishankara (2002), Quantum yields for production of O (^1D) in the ultraviolet photolysis of ozone: Recommendation based on evaluation of laboratory data, *J. Geophys. Res.*, *107*(D3), 4024, doi:10.1029/2001JD000510.

Merienne, M. F., A. Jenouvrier, and B. Coquart (1995), The NO_2 absorption spectrum: 1. Absorption cross-sections at ambient temperature in the 300-500 nm region, *J. Atmos. Chem.*, *20*, 281–297.

Shetter, R. E., et al. (2003), Photolysis frequency of NO_2: Measurement and modeling during the international photolysis frequency measurement and modeling intercomparision (IPMMI), *J. Geophys. Res.*, *108*(D16), 8544, doi:10.1029/2002JD002932.

Spirig, C., et al. (2005), Eddy covariance flux measurements of biogenic VOCs during ECHO 2003 using proton transfer reaction mass spectrometry, *Atmos. Chem. Phys.*, *5*, 465–481.

Stroud, C., et al. (2005), Role of canopy-scale photochemistry in modifying biogenic-atmosphere exchange of reactive terpene species: Results from the CELTIC field study, *J. Geophys. Res.*, *110*, D17303, doi:10.1029/2005JD005775.

Troe, J. (2000), Are primary quantum yields of NO_2 photolysis at $\lambda \leq$ 398 nm smaller than unity?, *Z. Phys. Chem.*, *214*, 573–581.

Volz-Thomas, A., A. Lerner, H.-W. Pätz, M. Schultz, D. S. McKenna, R. Schmitt, S. Madronich, and E. P. Röth (1996), Airborne measurements of the photolysis frequency of NO_2, *J. Geophys. Res.*, *101*, 18,613–18,627.

Webb, A. R., A. Kylling, M. Wendisch, and E. Jäkel (2004), Airborne measurements of ground albedo and cloud spectral albedos under low aerosol loads, *J. Geophys. Res.*, *109*, D20205, doi:10.1029/2004JD004768.

B. Bohn, R. Koppmann, and F. Rohrer, Institut für Chemie und Dynamik der Geosphäre II: Troposphäre, Forschungszentrum Jülich, D-52425 Jülich, Germany. (b.bohn@fz-juelich.de)